

Identification of moving train loads on railway bridge based on strain monitoring

Hao Wang^{*1}, Qingxin Zhu¹, Jian Li², Jianxiao Mao¹, Suoting Hu³ and Xinxin Zhao³

¹Key Laboratory of C&PC Structures of Ministry of Education, Southeast University, Nanjing, China

²Department of Civil, Environmental and Architectural Engineering, The University of Kansas, Lawrence, Kansas, USA

³Railway Engineering Research Institute, China Academy of Railway Sciences, Beijing, China

(Received July 4, 2018, Revised November 2, 2018, Accepted January 17, 2019)

Abstract. Moving train load parameters, including train speed, axle spacing, gross train weight and axle weights, are identified based on strain-monitoring data. In this paper, according to influence line theory, the classic moving force identification method is enhanced to handle time-varying velocity of the train. First, the moments that the axles move through a set of fixed points are identified from a series of pulses extracted from the second derivative of the structural strain response. Subsequently, the train speed and axle spacing are identified. In addition, based on the fact that the integral area of the structural strain response is a constant under a unit force at a unit speed, the gross train weight can be obtained from the integral area of the measured strain response. Meanwhile, the corrected second derivative peak values, in which the effect of time-varying velocity is eliminated, are selected to distribute the gross train weight. Hence the axle weights could be identified. Afterwards, numerical simulations are employed to verify the proposed method and investigate the effect of the sampling frequency on the identification accuracy. Eventually, the method is verified using the real-time strain data of a continuous steel truss railway bridge. Results show that train speed, axle spacing and gross train weight can be accurately identified in the time domain. However, only the approximate values of the axle weights could be obtained with the updated method. The identified results can provide reliable reference for determining fatigue deterioration and predicting the remaining service life of railway bridges.

Keywords: railway bridges; strain-monitoring data; moving train loads; identification; influence line

1. Introduction

Monitoring moving train loads, especially the extreme values of train loads, is one of the most important aspects for determining fatigue deterioration (Gu *et al.* 2014, Mori *et al.* 2007) and predicting the remaining service life of railway bridges (Yang *et al.* 2004, Kim *et al.* 2012). With the rapid development of monitoring techniques (Ou *et al.* 2010), numerous bridges are equipped with comprehensive structural health monitoring systems (SHMSs) worldwide (Wang *et al.* 2016, Xu *et al.* 2010, Ni *et al.* 2008), aiming to provide effective structural performance evaluation, damage detection, and safety assessment (Mao *et al.* 2017). For example, Spencer *et al.* (2015) used wireless smart sensors to develop a cost-effective and practical portable SHMS for railway bridges. Information offered by the SHMSs also enables characterization of the dynamic behaviors of the whole bridge and members (Zhao *et al.* 2016). Moreover, algorithms for early and fast warning of abnormal vibrations have also been developed based on the SHMSs, with the goal to ensure safe operation of these bridges (Ding *et al.* 2017, An *et al.* 2017).

However, capturing the interaction forces between the wheels and tracks directly is challenging, because the

moving force varies in time and space simultaneously (Pan *et al.* 2018). Therefore, it would be beneficial to develop indirect identification methods based on the known dynamic properties of bridges and the measured dynamic responses under moving loading. The bridge weigh-in-motion technology plays an important role in bridge health monitoring (Yu *et al.* 2007). Lydon *et al.* (2016) presented a general review on the BWIM theory and critical issues emerged in the current practices. Many methods have been proposed for moving force identification of bridges (Zhu and Law 2016, Yu *et al.* 2016). A method based on modal superposition was developed to identify the moving forces in the time domain using vibration responses caused by the forces (Law *et al.* 1997). Based on this technique, Law *et al.* (1999) proposed a time-frequency domain method, which is faster and provides results that are more accurate. Wu *et al.* (2010) proposed a moving force identification technique based on a statistical system model. Deng *et al.* (2010) proposed a moving force identification method for identifying the dynamic interaction forces using the superposition principle and the influence surface concept. Yu *et al.* (2017) proposed an identification method using wavelet analysis, which can accurately identify vehicle speed and axle spacing. Chan *et al.* (2001a, b) introduced four methods for determining dynamic axle loads from bridge responses. Numerical simulations and laboratory test results show that these methods are effective and accurate for identifying a set of moving loads. However, few of them are utilized to identify parameters of the moving train loads

*Corresponding author, Professor
E-mail: wanghao1980@seu.edu.cn

with time-varying velocity based on field measurement. Based on the finite element method or modal decomposition, several methods have been proposed to identify the axle loads travelling with non-uniform speed, (Law *et al.* 2004, Zhu *et al.* 2003, Chan *et al.* 2001). However, these methods face challenges when identifying the parameters of the trains with dozens of axles, for the necessity of accurate bridge models and their high computational demand.

Influence lines are a generally accepted method to describe the quasi-static properties of structures, which comprehensively reflect the boundary conditions, geometric properties, and material properties of a structure (Wang *et al.* 2014). Laboratory studies demonstrate that influence lines can be extracted if the bridge response, which is a function of vehicle location, axle spacing, and axle weight, is known (Catbas *et al.* 2011). Zaurin *et al.* (2009, 2011) demonstrated the integration of video images and sensor data as promising techniques to obtain unit influence line (UIL) as a bridge safety index. In addition, Sun *et al.* (2016) demonstrated strain influence lines can provide reasonable assessment of bridge health condition at least in the vicinity of strain monitoring points. Based on influence lines, several modified algorithms aiming to capture parameters of vehicles have been proposed (Zhao *et al.* 2013, Marques *et al.* 2016). Meanwhile, strain is one of the most commonly measured responses in structural monitoring (Doebeling *et al.* 1998, Mao *et al.* 2018a, b). Deng *et al.* (2015) presented a case study on fatigue performance assessment of welded details based on long-term strain monitoring data. Ni *et al.* (2011) proposed a structural condition assessment method for the cable-stayed bridge deck of Tsing Ma Bridge based on long-term strain monitoring data. Therefore, combining strain monitoring data and the concept of influence lines, in this paper, an enhanced influence-line-based method aiming to identify the moving train load parameters is presented.

In this study, an identification method of moving train load parameters is proposed based on the basic theories of strain influence line, which account for the effect of time-varying train velocity. Then, numerical simulations are employed to verify the proposed method and investigate the effect of the sampling frequency on the identification accuracy. Subsequently, the proposed method is applied to a continuous steel truss railway bridge for extracting the moving train load parameters, using field measured train-induced strain data. In addition, the identification results are compared with direct measurements. The proposed method does not require development of the bridge model or influence lines. The uniqueness of the proposed method is the non-intrusive calculation of train characteristics which requires only the strain measurements. The enhanced method is computationally more efficient, and easier to implement in field.

2. Theoretical formulation for moving train loads identification

This section illustrates the proposed method using the

strain responses of a simply supported beam excited by a series of moving forces with fixed spacing. The proposed method considers the train speed in the axle weights calculation to eliminate the error caused by the time-varying train speed. The strain measurements of railway bridge members are utilized to determine train speed, axle spacing, gross train weight and axle weights with the proposed method. Note that the bridge model is not required.

2.1 Influence line theory

A series of moving forces with fixed spacing along a simply supported beam is used to represent the moving train loads on the bridge. The schematic, representing a single span bridge with a single axle load, is shown in Fig. 1.

The equation of the strain response at the bottom of mid-span point, C, is given by (Long and Bao 2001)

$$\varepsilon = \begin{cases} \frac{Pxy}{2EI} & 0 \leq x \leq L/2 \\ \frac{PLy}{2EI} \left(1 - \frac{x}{L}\right) & L/2 < x \leq L \end{cases} \quad (1)$$

where ε is the strain underneath point C, P is the magnitude of the point load, x is the distance from A to the location of the point load, y is the distance from the sensor location to the centroid of the cross-section, I is the moment of inertia of the cross-section, E is the modulus of elasticity, and L is the total length of the beam.

If discrete samples of the strain are recorded at a distance interval Δx , the second derivative of the strain data with respect to the distance, x , can be written as Eq. (2). Note that a series of pulses could be observed from the second derivative values when the axle load enters the span, crosses the middle of the span, and leaves the span. The positive peaks correspond to the entering and leaving time of the point load, respectively, while the negative peak corresponds to the time that the point load crosses the middle of the span. In addition, the negative peak of the second derivative is twice as large as the positive peak.

$$\frac{d^2\varepsilon}{dx^2} = \begin{cases} \frac{Py}{2EI\Delta x} & x = 0 \text{ or } L \\ -\frac{Py}{EI\Delta x} & x = L/2 \\ 0 & \text{elsewhere} \end{cases} \quad (2)$$

However, the strain responses are recorded at a time interval, Δt , rather than a distance interval, Δx . The distance, x , can be converted into time, t , as $\Delta x = \sum v(t) \cdot \Delta t$, in which $v(t)$ is the moving speed of the point load.

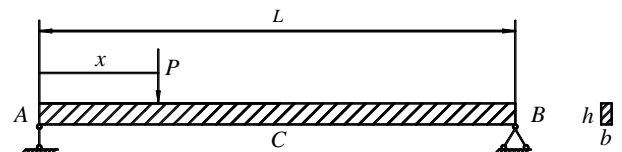


Fig. 1 Simply supported beam with a point load

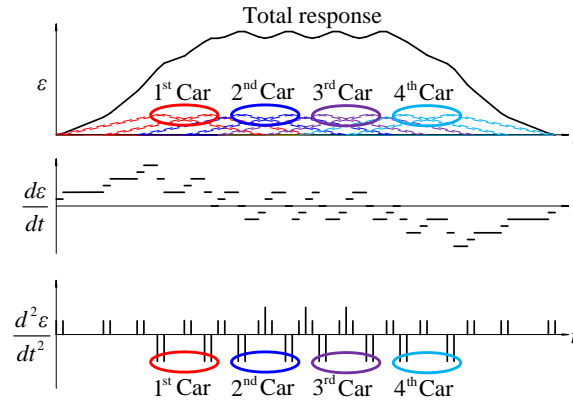


Fig. 2 Strain response and associated derivatives for a typical four-car train

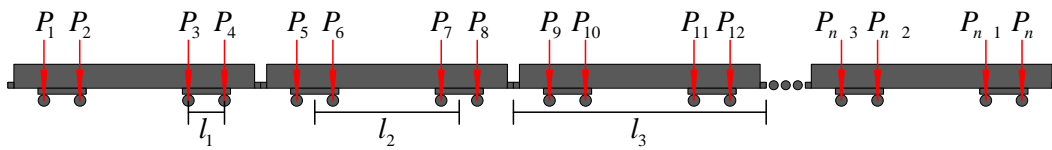


Fig. 3 The train model

The axle speed is considered constant for the short distance, Δx . Therefore, the equation, $\Delta x = \sum v(t) \cdot \Delta t$, could be written as $\Delta x = \sum v \cdot \Delta t$, when the axle crosses the fixed point. The velocity variation is considered small enough to be neglected. Hence, the second derivative of the strain measurement can be written as Eq. (3), where t_e is the time that the point load leaves the span. The peak values of the second derivative with respect to time are closely related to the magnitude of the point load, P , the instantaneous speed, $v(t)$, and sampling time interval, Δt .

$$\frac{d^2\varepsilon}{dx^2}(t) = \begin{cases} \frac{Pyv^2(t)}{2EI\Delta t} & t = 0 \text{ or } t_e \\ -\frac{Pyv^2(t)}{EI\Delta x} & t = t_m \\ a \text{ small value} & \text{elsewhere} \end{cases} \quad (3)$$

The strain and associated derivatives at any location along the length of the beam will take the same form as Eqs. (1)-(3), with reduced amplitudes. Superposition can be used to account for more than one axle. For a typical four-car train running on a simply supported beam, the strain response and associated derivatives are shown in Fig. 2. The axle weights are identical and the train travels at a constant velocity. Fig. 3 illustrates the axle spacing.

2.2 Train parameter identification

According to the properties of the influence line, the train speed and axle spacing can be obtained based on the moments that the axles move through a set of fixed points. In addition, the integral area of the measured strain data reveals the gross train weight, while the second derivative peaks of the strain data reveal the relative amplitude of the axle weights.

2.2.1 Train speed

The second derivative of the strain data exhibits pulses when axles enter the span, cross the middle of the span, and leave the span (Fig. 2). The train speed could be determined by the time duration when the axle passes two of these locations. Note that when axles pass over the middle of the span, the negative peaks of the second derivative are twice as large as the positive peaks (Fig. 2). Therefore, combining the moments in time when the axles pass mid-spans of two adjacent spans allows for speed calculation of the train crossing a continuous beam bridge. With the traveling time obtained from the difference between the two moments in time, the train speed can be calculated with the traveling distance l , namely, the axle speed as $v_n = l / \Delta t_n$, where v_n is the speed of the n^{th} axle (m/s), l is the distance between the two fixed points (m) and Δt_n is the traveling time of the n^{th} axle (s).

2.2.2 Axle spacing

The second derivative of strain response (Fig. 2) provides the moments when the axles pass the mid-span of the bridge. The durations between these time points provide the axle spacing, TL_n , in conjunction with the calculated instantaneous velocity, $v(t)$. The axle spacing can be calculated as $TL_n = v(t_{n+1} - t_n)$, where TL_n is the distance between the n^{th} and $(n+1)^{\text{th}}$ axles, and t_n is the time that the n^{th} axle takes to reach the mid-span of the bridge after the first axle reaches the mid-span.

2.2.3 Gross train weight

The integral area of the strain response induced by a unit force moving on a bridge with a unit speed, can be written as

$$ILA = \sum \varepsilon(t)/f \quad (4)$$

where f is the sampling frequency of the strain data. Subsequently, the gross train weight of each train can be obtained by

$$GTW = \frac{A_s}{v \cdot ILA} \quad (5)$$

where A_s represents the integral area of the measured strain data under the moving train load, v is the average velocity. The error induced by the slight variation of train velocity is ignored. Note that this method does not account for the dynamic amplification effect of the bridge response.

2.2.4 Axle weights

The point loads are assumed to be equivalent to the axle weights. According to Eq. (3), the point loads are determined by the gross train weight, the second derivative of the strain measurements and the axle speeds. The axle weights can be obtained as

$$P_n = \left[\frac{\frac{d^2\varepsilon}{dt^2}(n) \frac{1}{v_n^2(t)}}{\sum_{i=1}^N \frac{d^2\varepsilon}{dt^2}(i) \frac{1}{v_i^2(t)}} \right] \times GTW \quad (6)$$

where P_n is the weight of the n^{th} axle. The peak values of the second derivative of the strain are divided by axle speeds twice to handle time-varying velocity of the train. Subsequently, the gross train weight is distributed by the corrected peak values. Therefore, the identification accuracy of axle weights is affected by the calculation accuracy of gross train weight, axle speeds and peak values of second derivative.

3. Numerical simulations

A simply supported beam subject to a series of moving forces is used to represent the generic train-bridge system, aiming to: (a) investigate the characteristics of the vibration induced by moving trains, (b) verify the proposed method and investigate the effect of the sampling frequency on identification accuracy, and (c) select the cut-off frequency of the low-pass Butterworth filter to remove the dynamic components.

However, the limitations of numerical model of bridge in ideal condition would affect the results of simulations: (a) the static deflection caused by the bridge self-weight is not considered in the simulation analysis, (b) the numerical modeling of bridge does not account for the dynamic response induced by vehicle-bridge coupled vibration, and (c) the requirements of superposition are coordinated well with the numerical model. Hence, the identification accuracy of numerical model would be better than that of real bridges.

3.1 Bridge model and vehicle model

A simply-supported steel bridge, which has a uniform

cross-section, is adopted for the simulation. The design span and cross-section are shown in Fig. 1, in which the bridge span is 30 m, and the beam is 1.0 m in height and 0.5 m in width. The mass per unit length of the bridge is 3925 kg/m, the moment of inertia of the cross-section is $4.17 \times 10^{-2} \text{ m}^4$, and the modulus of elasticity is $2.06 \times 10^{11} \text{ Pa}$. Meanwhile, the multiple carriages are modeled by a series of moving force with fixed spacing. Fig. 3 illustrates schematically the generic train model. The train is composed of 10 carriages with 20 bogies and 40 wheel-sets in total, the static axle loads for the carriages are around 16t, and the design train speed is 6m/s. Carriage geometry is described using the carriage length ($l_3=25$ m), bogie spacing ($l_2-l_1=14$ m) and axle spacing ($l_1=2$ m).

3.2 Natural frequencies

3.2.1 Natural frequencies of bridge

The mass and span of the bridge determine the vertical and lateral natural frequencies of the bridge. The equation can be written as (Milne *et al.* 2017)

$$f_i = \frac{n^2\pi}{2L^2} \sqrt{\frac{EI}{\rho A}} \quad (7)$$

where f_i is the i_{th} mode natural frequency of the structure, ρA is the mass per unit length.

3.2.2 Driving frequencies

Moving trains produce significant vibrations of bridges, thus, many studies have been conducted on the characteristics of the dominant vibration induced by moving trains (Ju *et al.* 2009, Lu *et al.* 2012, Milne *et al.* 2017) and the resonant vibration characteristics of vehicle-bridge system when trains pass bridges (Ju *et al.* 2003, Xia *et al.* 2006). The load function $P(t)$ represents a sequence of axle loads, which can be obtained as

$$P(t) = \sum P_n \delta(t - t_n) \quad (8)$$

where δ is the Dirac delta function, the Fourier transform of Eq. (8) describes the frequency content of the loads. The load spectrum depends on the geometry of the train, the relative amplitudes of the wheel loads and the train speed. It is challenging to describe the vibration characteristics induced by trains with time-varying velocities using the formulas. An infinitely long train that consists of identical repeating vehicles, moving with constant velocity, v , is considered. The train load function can be written as a Fourier series

$$P(t) = \sum_{N=-\infty}^{\infty} U_N e^{-i2\pi Nvt/l_3} \quad (9)$$

where the Fourier series coefficients depend on the vehicle geometry and wheel load, P .

$$U_N = 4P \frac{v}{l_3} \cos\left(\frac{\pi N l_1}{l_3}\right) \cos\left(\frac{\pi N l_2}{l_3}\right) \quad (10)$$

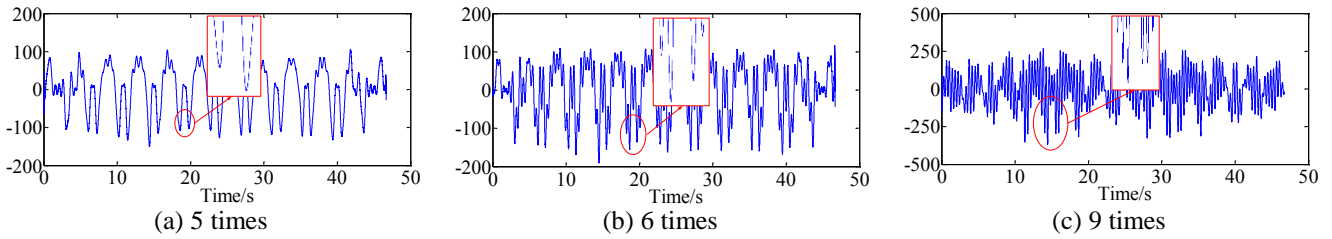


Fig. 4 The calculation results based on different cut-off frequencies

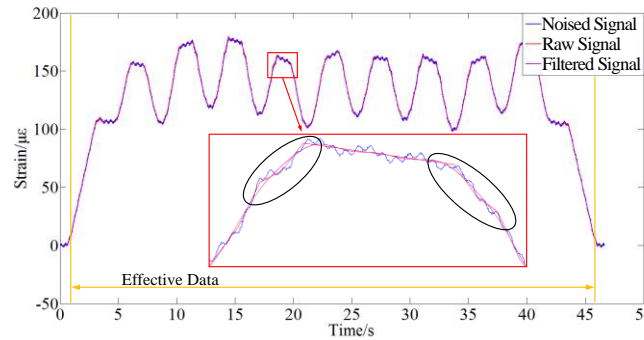


Fig. 5 Comparison between the raw and filtered strain

Note that the frequencies of loading only exist at integer multiples of the vehicle passing frequency. The amplitudes of these discrete frequencies are the Fourier series coefficients, U_N , evaluated over one period of the train, l_3/v .

3.2.3 Natural frequencies of train-bridge system

When a train moves on a bridge, the frequencies of the bridge will be affected due to the effects of train mass coupled with the bridge through the suspension systems. The natural frequencies of the bridge during the passage of a train may be established based on the dynamic equation for the bridge coupled with the moving train, as follows (Lu *et al.* 2012)

$$\rho A \frac{\partial^2 z}{\partial t^2} + EI \frac{\partial^4 z}{\partial x^4} + c \frac{\partial z}{\partial x} = P(x, t) \quad (11)$$

where c is the damping coefficient of the bridge, z is the bridge vertical displacement, and $P(x, t)$ is the contact force between the carriage and the bridge. For a simply supported bridge, the numerical integration method can be employed to obtain the bridge natural frequencies at each time step.

3.3 Simulation results

The strain response at the bottom of mid-span point, C , is shown in Fig. 5, which consists of all the frequencies and white noise. The white noise level is 5% of the root mean square (RMS) of the dynamic strain response induced by the 10-carriage train, and the frequency band is 0.1Hz ~ 100Hz. Note that the static deflection caused by the bridge self-weight is not considered in the analysis.

The proposed method is based on structural static responses induced by moving train loads. Therefore, the dynamic components need to be removed from the response measurements in advance. A low-pass Butterworth filter is

applied to eliminate the dynamic strain and noise. When the cut-off frequency is selected as six to eight times of the fundamental frequency of the train load, the peaks of the second derivative of strain measurements can be clearly identified. The second derivatives of strain data with different cut-off frequencies are shown in Fig. 4. The static strain component is distorted seriously during the filtering when a lower cut-off frequency is selected. Furthermore, the dynamic components and white noise can not be removed effectively when a higher cut-off frequency is selected. The peaks of the second derivative, which are induced by axle loads, can be identified from Fig. 4(b). However, that can not be obtained from Fig. 4(a) and (c). The raw strain and the filtered data based on a proper cut-off frequency are compared in Fig. 5.

3.4 Effect of sampling frequency

The large errors could occur due to the relatively low sampling frequency. To investigate the effect of sampling frequency on the identification accuracy, three sampling frequencies, i.e., 100Hz, 250Hz and 500Hz, are used to record the strain response.

Based on the time durations of the pulses extracted from the second derivative of the structural strain response, the carriage geometries, including axle spacing, bogie spacing and carriage length, could be obtained, which are shown in Fig. 6. The ‘‘Standard’’ means the exact value. The identification results of the axle spacing under the bogie are larger than the exact values. Meanwhile, the identification results of the bogie length and carriage length match well with the exact values. Namely, it is hard to identify the moments precisely when two close axles cross the fixed point, since the static strain component is distorted during the filtering, as shown in Fig. 5. In addition, the errors

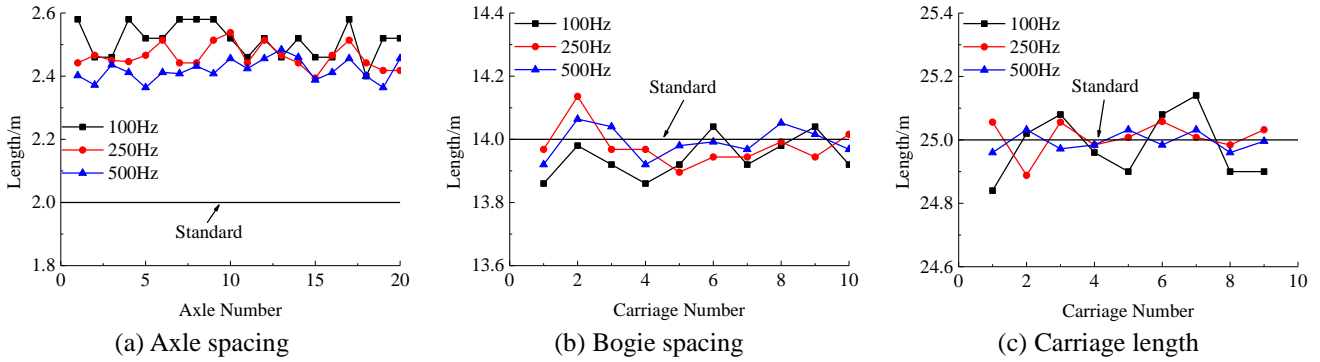


Fig. 6 The carriage geometries

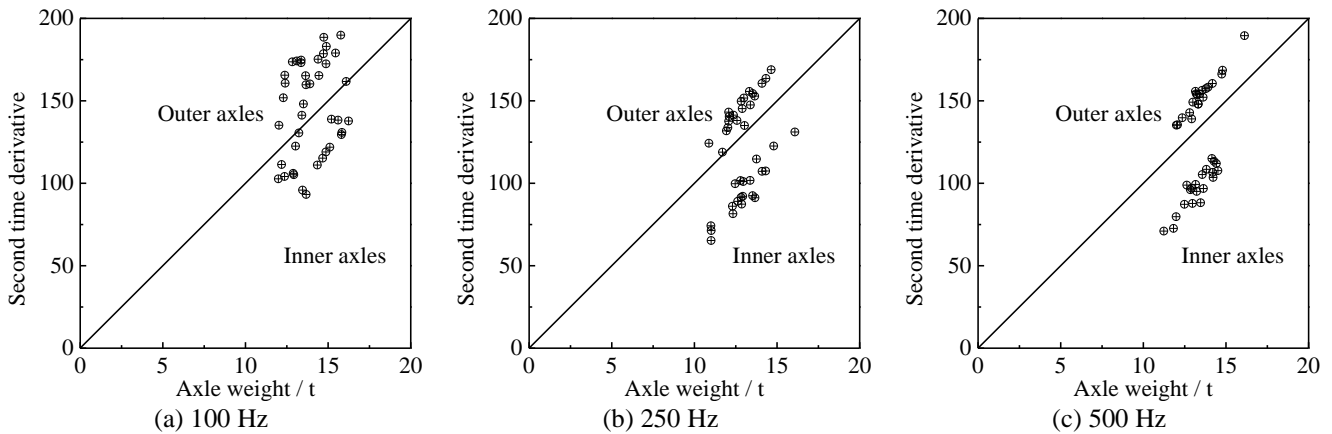


Fig. 7 The second derivative values corresponding to axle weights

decrease with the increase of axle spacing.

The identification results using strain data recorded by the sampling frequency 500 Hz are more accurate than the others, namely, the sampling frequency of the data acquisition system has influence on the identification accuracy. The accuracy of the moment when the axle crosses the fixed point is affected by the sampling frequency. Specifically, the accuracy of the identification results of axle speed and carriage geometries increase with the increase of sampling frequency. However, the accuracy does not keep increasing after the sampling frequency exceeded a particular value.

The axle weights and peak values of the second derivatives of the strain data recorded by the sampling frequencies 100Hz, 250Hz and 500Hz are shown in Fig. 7. It can be seen that the peaks corresponding to outer axles and inner axles show different linear relationship with the axle weights, due to the filtering process. However, the ratio of peak values of inner axles to peak values of outer axles is a constant, which is related to sampling frequency. Hence, the peak values of inner axles or outer axles should be corrected to eliminate the difference induced by the filtering process. In addition, the sampling frequency of the data acquisition system has significant influence on the identification accuracy, the higher sampling frequency increases the identification accuracy.

4. Case study

The proposed methodology is applied to field measurement data on a continuous steel truss railway bridge. The complexity of real bridge situation may create challenges in train load identification.

4.1 Engineering background

4.1.1 Description of the railway bridge

The Xiangtan Bridge (Fig. 8) investigated in this study is a linkage connecting the cities of Kunming and Shanghai (Fig. 9), which is about 844.15 m long and consists of 11 simply supported bridge spans. As illustrated in Fig. 7, these bridge spans are arranged as 49.86 m+72.8 m+3×75 m+ 6×72.8 m+35 m+12.8 m. Among the 11 bridge spans, ten of them are steel truss bridges and the other is steel-plate girder bridge. As shown in Fig. 10, the spans named as G1 and G5 to G10 are truss bridges with the railway at the top chord (deck truss). The lengths of these spans are 72.8 m, and the trusses are 9.5 m in height and 3 m in width. The spans G2, G3, and G4 are navigable spans, therefore, these truss bridges have the railway at the bottom chord. The lengths, heights and widths of these spans are 75.0 m, 10.0 m and 5.8 m, respectively. The span G11 consists of a steel-plate girder bridge with two main girders connected by cross frames. The height of this girder bridge is 3.28 m and the width is 2.0 m.



Fig. 8 A photo of the Xiangtan railway bridge



Fig. 9 An aerial view of the bridge

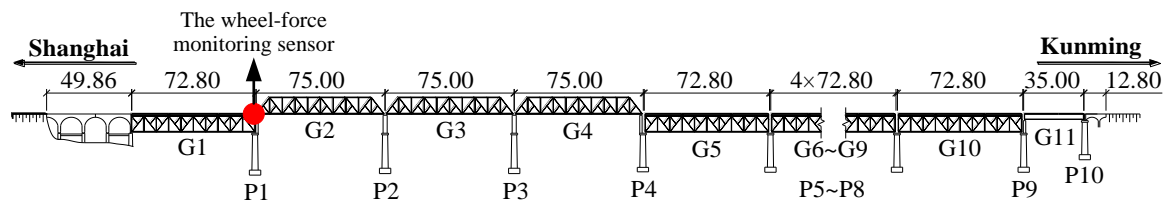


Fig. 10 A schematic view of Xiangtan bridge (Unit: m)

4.1.2 Description of the SHMS

To ensure the safety, durability, and serviceability of the Xiangtan Bridge under long-term heavy train loads, a comprehensive SHMS has been installed for performance assessment. Both structural responses and operational conditions, including displacement, acceleration, strain, temperature and traffic loads, are monitored. The SHMS was installed on March 2016 and has been operating since then. A large amount of data under service conditions has been collected. The monitoring data used in this study is mainly collected by sensors installed on spans G1 and G2. Fig. 11 presents the sensor layout. Typical sensor installations are shown in Fig. 12, including accelerometer, displacement sensor, strain gauge and temperature meter. The strain gauge specifications are shown in Table 1. In addition, a pair of wheel-force monitoring sensors, as shown in Figs. 10 and 13, is symmetrically installed on the tracks at the connection of G1 and G2. The sensor is developed by China Academy of Railway Sciences and can accurately record the contact forces between the track and

train wheels. Meanwhile, the train velocities, corresponding to the first carriage crossing the connection of G1 and G2, are recorded (Tao *et al.*). During the measurement, the sampling frequencies of all the sensors are set to 205Hz. The duration of the measurements depends on the train type and the time when sensors are triggered to take data.

4.2 Recorded structural responses

The bridge is subject to a wide range of external loads during its lifetime, including temperature, wind, traffic loads, earthquake, and impact loads, which induce both static and dynamic responses of the bridge. The proposed method, however, is based on structural static responses induced by moving train loads. Therefore, the dynamic components need to be removed from the response measurements in advance. Fig. 14 presents typical vibration responses induced by the moving train loads. It can be observed that the strain and acceleration responses of the bridge significantly increase at the beginning and the

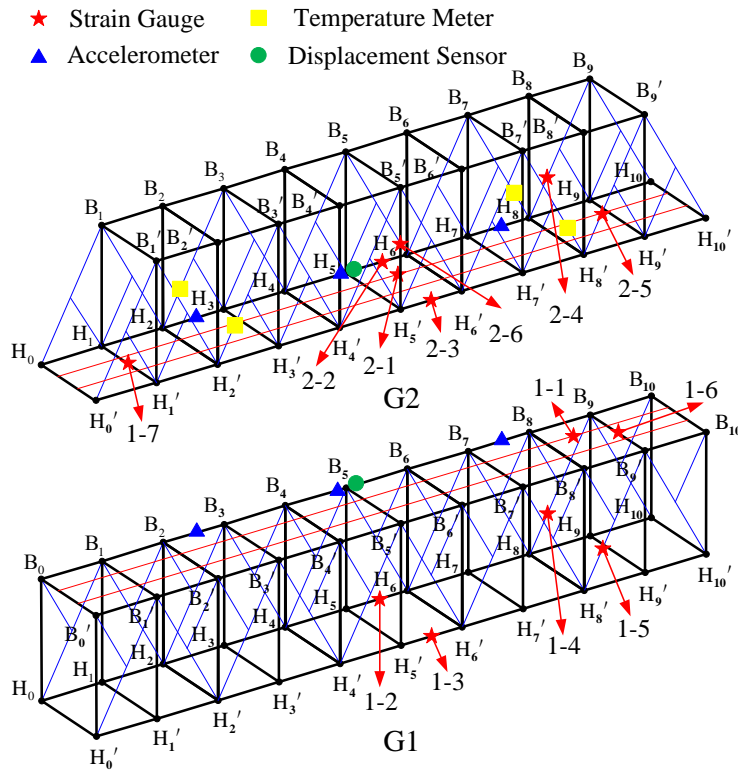


Fig. 11 Sensors layout of the SHMS



(a) Accelerometer



(b) Displacement sensor



(c) Temperature meter



(d) Strain gauge

Fig. 12 Typical sensors

locomotive is heavier than the carriage. The power spectral densities (PSDs) of the recorded strain and acceleration data are shown in Fig. 15. The strain components at low frequency are dominant according to the energy distribution. Meanwhile, there are observable peaks at higher frequencies corresponding to the structural vibration modes, which can be confirmed with reference to the PSD of the acceleration. Moreover, noise components can be observed across all frequencies.

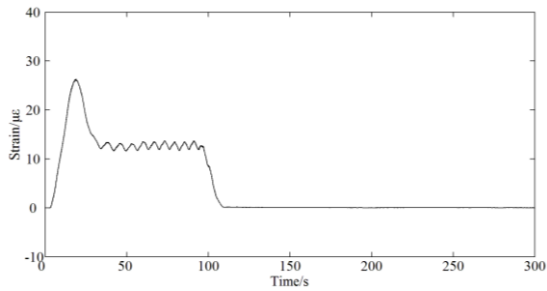
Ambient temperature and wind load usually have significant effects on structural static strain. The baselines of sensors were calibrated to remove the temperature effect before the data was recorded. On the other hand, the wind speed at the bridge site is less than 3 m/s. Therefore, the wind effects are considered small enough to be neglected. To extract the static strain from the raw strain measurement, a low-pass filter is applied to eliminate the dynamic strain as well as noise. The comparison between the raw strain and the filtered data is shown in Fig. 16.

Table 1 Strain sensor specifications

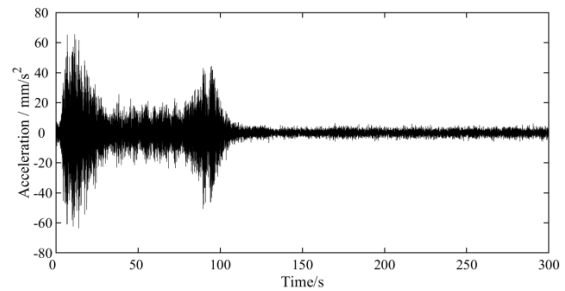
Range	Working Temperature	Resolution	Temperature Drift
0~2000 $\mu\epsilon$	-20~65 $^{\circ}\text{C}$	0.2 $\mu\epsilon$	-0.019 $\mu\epsilon/^{\circ}\text{C}$



Fig. 13 The wheel-force monitoring sensor



(a) Recorded strain data at measurement point 1-2



(b) Vertical acceleration at the mid-span of G1

Fig. 14 Recorded structural responses under moving train loads

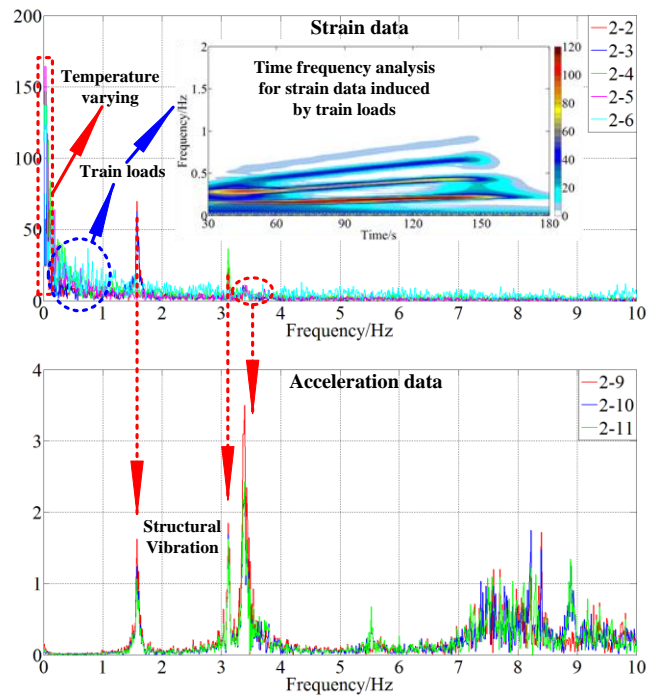


Fig. 15 PSDs of strain and acceleration data

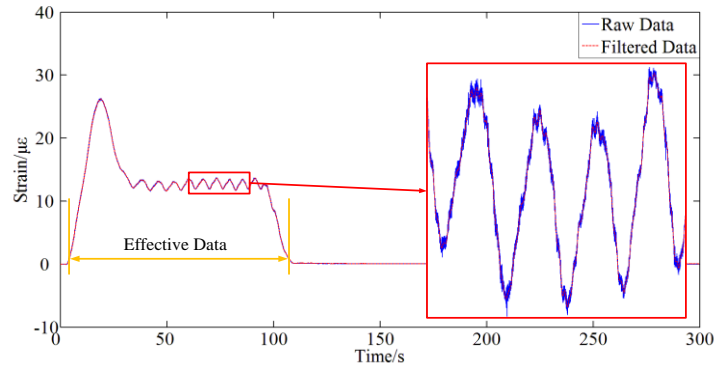


Fig. 16 Comparison between the raw and filtered strain

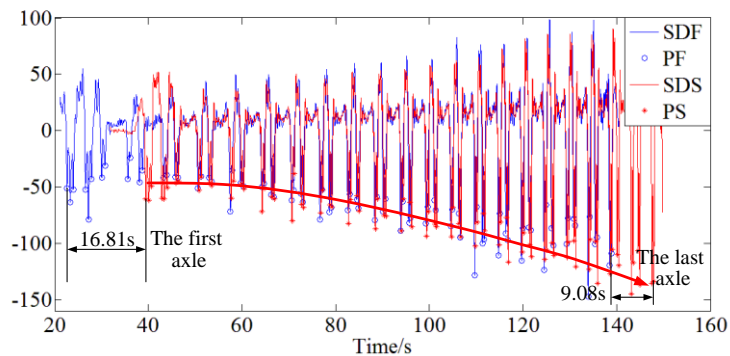


Fig. 17 The second derivatives of the strain measurements

4.3 Identification of train parameters

About 110 trains pass over the bridge every day. Several of them were randomly selected to verify the proposed method. The detailed information of these train events is shown in Table 2. The “Train speed” represents the instantaneous velocities recorded by the SHMS. The train events 4, 5 and 6 were selected as standard train events, while the other train events were used to validate the proposed method by comparing the calculated moving train load parameters with the measured values. The structural properties of Xiangtan Bridge would not change in several months obviously. Hence, the standard train events were selected randomly, aiming to: (a) calculate the integral area of the strain response induced by a unit force moving on the bridge with a unit speed, *ILA*, which is necessary for the gross train weight calculation, as described in section 2.2.3, and (b) calculate the correction ratio of inner axles or outer axles, as shown in Fig. 7, which is used to eliminate the differences induced by the filtering process.

The strain data of the measurement points 1-1 and 2-1 (Fig. 11) are selected to identify the moving train load parameters, which are subsequently validated by the recorded train speed, gross train weight and axle weights. The approximate values of the train speed and carriage length could be obtained based on the proposed method with the raw strain data. Then, the raw strain data is filtered according to the estimated train speed and carriage length, to extract the strain of the bridge members induced by the

moving train loads. Afterwards, the 5% of the maximum strain data is selected as the threshold to extract effective data as shown in Fig. 16. The processed data is selected to identify the moving train load parameters.

4.3.1 Train speed

The second derivatives of the measured strain data from the two selected measurement points are shown in Fig. 17. SDF and SDS represent the second derivatives of the strain data from measurement points 1-1 and 2-1, respectively. PF and PS represent the peaks of the second derivatives of the strain data from measurement points 1-1 and 2-1, respectively.

The axle speed of all the selected train events could be calculated based on the time duration when the axle passes the two locations. For example, the duration for the first axle and last axle are 16.81s and 9.08s, respectively. The distance between the two measurement points is 44.78 m, hence the velocity of the first and the last axle are 2.66m/s and 4.93 m/s, respectively. Subsequently, the axle speeds of the selected train events are shown in Fig. 18. All the speeds are increasing slightly when trains move on the bridge. As shown in Fig. 9, the trains are bound from Xiangtandong Station to Xiangtan Station. There are several curve lines between Xiangtandong Station and Xiangtan Bridge. Hence, the trains pass the region with low velocities. Then, the trains move forward with normal velocities.

Table 2 Information of train events

Train events	Time	Carriages number	Axle number	Train weight (t)	Train speed (km/h)
1	2016-03-24 10:30:38	16	70	971.19	19
2	2016-04-03 06:21:40	16	70	1035.08	10
3	2016-04-06 00:29:19	18	78	1050.57	15
4	2016-04-18 07:06:11	18	78	1149.28	18
5	2016-05-07 00:16:19	15	66	980.70	10
6	2016-05-11 00:40:51	18	78	1072.07	10
7	2016-05-20 01:10:43	12	54	737.26	8
8	2016-05-26 21:31:06	12	54	749.00	10
9	2016-09-02 08:18:18	19	82	1183.52	10

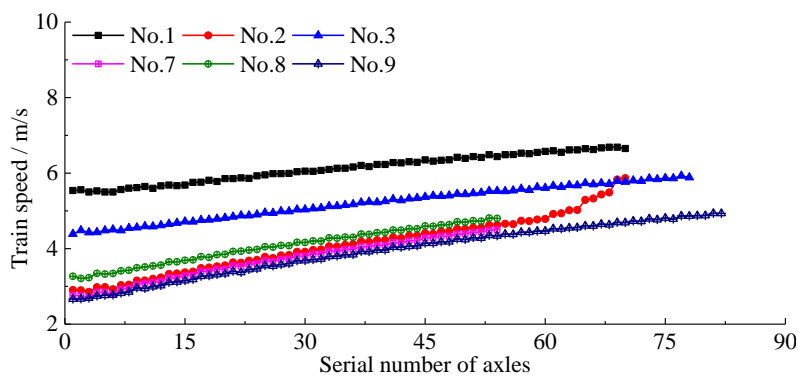


Fig. 18 The speeds of all axles

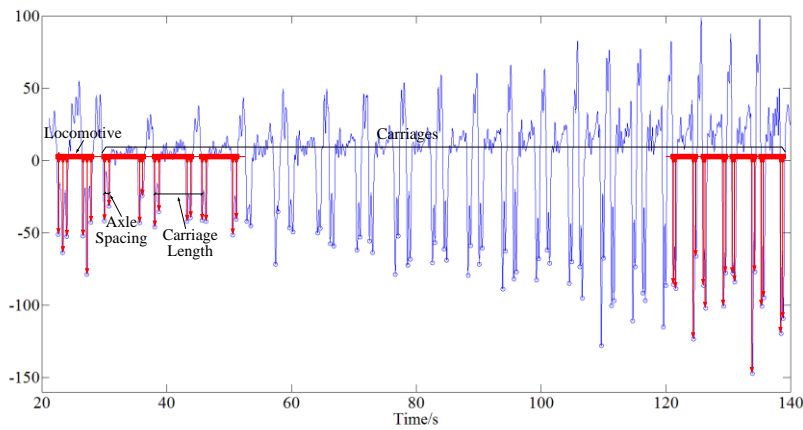


Fig. 19 Calculation of carriage geometries

4.3.2 Axle spacing

Fig. 19 illustrates the second derivatives of the strain data from the measurement point 1-1. There are three axles under the bogies of locomotive and two axles under the bogies of carriages. Both the locomotive and carriage are supported by two bogies. Hence, the first six peaks are induced by the axles under the locomotive, whereas other peaks are induced by the axles under carriages.

The axle spacing and carriage length can be obtained based on the calculated axle speeds and the durations of the axles passing the fixed location. As shown in Fig. 19, the

axle spacing under the same bogie can be obtained based on the time durations of the close peaks. For example, the time duration for the first two axles, which are under the front bogie of the first carriage, is 0.66s, and the speed of the first axle is 2.82 m/s. Hence, the axle spacing is calculated as 1.86 m. Meanwhile, the carriage length can be obtained on basis of the time durations of the peaks induced by the axles at the same position of the adjacent carriages. For example, the time duration for the first axles under the first and second carriages is 8.14s, and the speed of the first axle under the first carriage is 2.82 m/s. Hence, the carriage

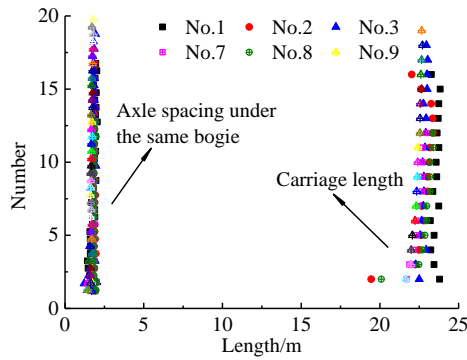


Fig. 20 The axle spacing and carriage length

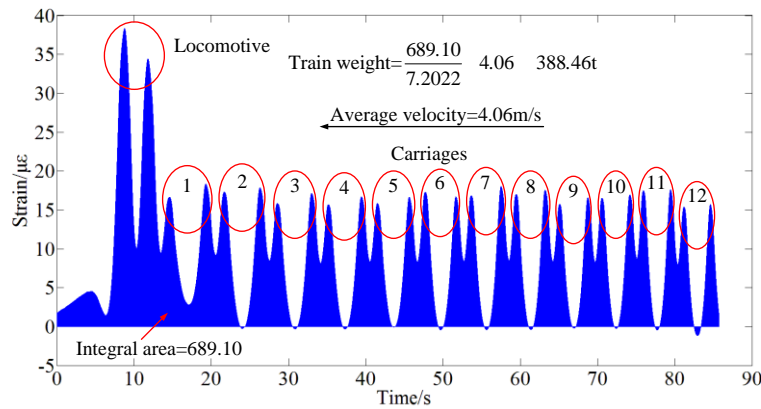


Fig. 21 Effective strain data induced by train event 8

Table 3 Calculation of train weights

Train events	Integral area 1 ($\mu\epsilon \cdot t$)	Integral area 2 ($\mu\epsilon \cdot t$)	Average speed (m/s)	Identified train weight 1 (t)	Identified train weight 2 (t)	Directly measured train weight (t)
1	209.00	591.89	6.12	918.64	1005.90	971.20
2	362.25	886.33	4.09	1064.10	1006.66	1035.08
3	260.56	698.96	5.21	974.98	1011.24	1050.56
7	281.14	720.41	3.68	743.06	736.20	737.26
8	267.10	689.10	4.06	778.84	776.92	749.00
9	421.08	1044.16	3.93	1188.52	1139.52	1183.52

length is calculated as 22.95 m. The identified carriage parameters, including axle spacing under the same bogie and carriage length, are shown in Fig. 20. The axle spacing under the same bogie is about 1.8m, and the carriage length is around 22.7 m. Both of the identification results match well with the actual values.

4.3.3 Train weight

Fig. 21 illustrates the effective strain data from the measurement point 2-1, which was induced by the train event 8. Based on the information of the standard train events, the integral areas of the strain data from the measurement points 1-1 and 2-1, which are both induced by a unit force crossing the bridge at a unit speed, are $1.3924 \mu\epsilon \cdot t$ and $3.6011 \mu\epsilon \cdot t$, respectively. As a result, the summation of the integral areas of the strain data, which is

shown in Fig. 21, is $689.10 \mu\epsilon \cdot t$. Since the average speed of the train event 8 is 4.06 m/s, according to Eq. (5), the gross train weight is calculated as 776.92t. As a reference, the direct measurement of the gross train weight is 749.00t. Table 3 lists the identification results of the selected train events along with the direct measurements. In Table 3, Integral area 1 and Integral area 2 represent the integral area of the strain data from measurement points 1-1 and 2-1, respectively. Identified train weight 1 and Identified train weight 2 represent the calculation results based on Integral area 1 and Integral area 2, respectively. Note that the identification results match well with the direct measurements. In other words, the error induced by the slight time-varying train velocity is negligible.

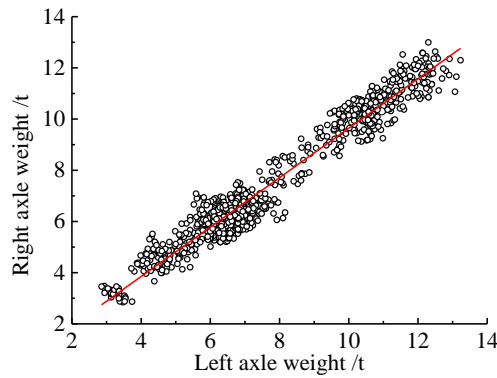


Fig. 22 Axle weight of trains

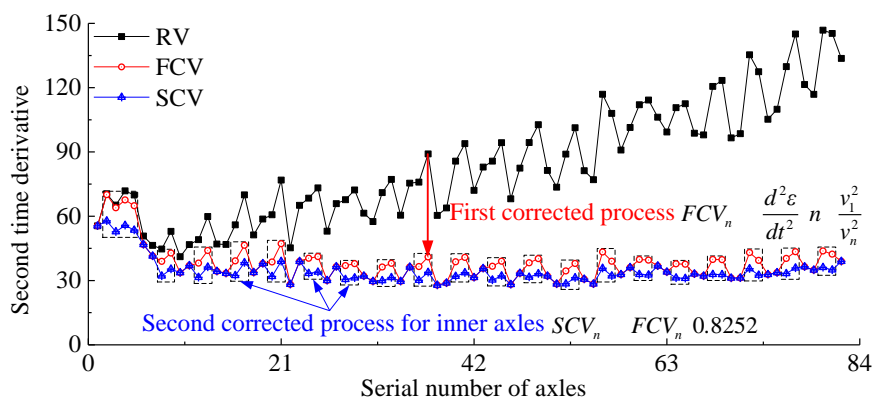


Fig. 23 The peak values of second derivative and corrected values

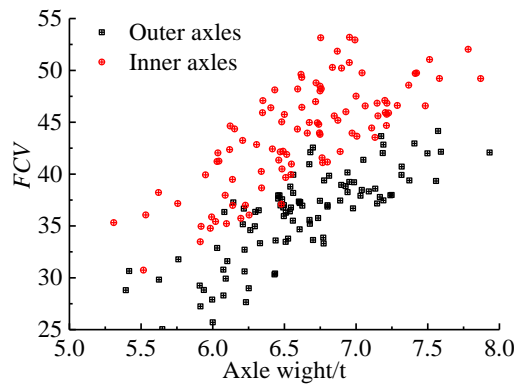


Fig. 24 The FCV corresponding to axle weights

4.3.4 Axle weights

The trains in this study are supported by two tracks. As shown in Fig. 22, there is a linear relationship between the left axle weight and the right axle weight. Hence, the tilt effect is neglected in this study. The calculated axle weight is equal to the sum of the left axle weight and the right axle weight.

The axle weights are identified according to Eq. (6). Fig. 23 illustrates the correcting process of the peak values of the second derivative from the measurement point 2-2, which were induced by the train event 9. In Fig. 23, *RV*

represents the peak values of the second derivatives, *FCV* and *SCV* represent the first corrected values and second corrected values, respectively.

The train speeds, which are shown in Fig. 17, were increasing when trains were passing across the bridge. According to Eq. (3), the parameter, $y/EI\Delta t$, is constant during the train parameters calculation. Thus, there is a direct linear relationship between the axle loads and the parameter, $d\epsilon^2/(dt^2 \times v_n^2)$. The v_1^2 , which is calculated based on the velocity of the first axle, is a constant value.

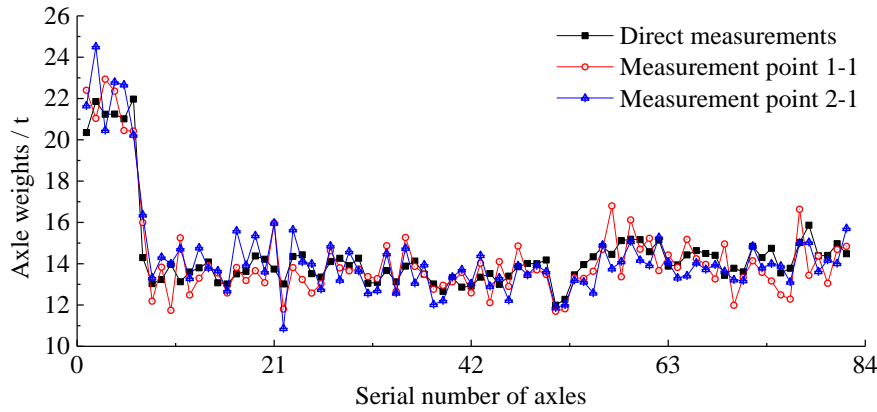


Fig. 25 The identification results and direct measurements of axle weights

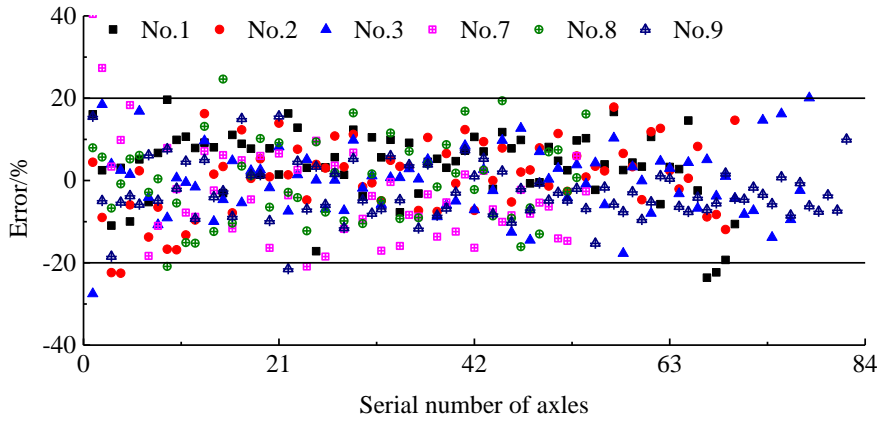


Fig. 26 The errors of the calculation results of axle weights

Accordingly, the second derivate is multiplied by v_1^2/v_n^2 to obtain the first corrected value (*FCV*), in which the effect of time-varying velocity is eliminated. Subsequently, according to Fig. 7, the peak values of inner axles or outer axles were corrected again to eliminate the difference induced by the filtering process. Based on the standard train events, the relationship between the *FCV* and the axle weights is shown in Fig. 24. The corrected parameter, *IF*, of the peak values of inner axles is obtained by the Eq. (12).

$$IF = \frac{1}{n} \left(\sum \frac{AWI_i}{FCVI_i} \cdot \frac{FCVO_i}{AWO_i} \right) \quad (12)$$

where n represents the amount of bogies under the standard trains. *AWI* and *AWO* represent the recorded axle weights of inner axles and outer axles, respectively. *FCVI* and *FCVO* represent the *FCV* of inner axles and outer axles, respectively. The *IF* of inner axles is 0.8252 herein.

As shown in Table 3. The calculation result of train weight from the measurement point 2-1 is 1139.52t. The identified train weight was distributed by the second corrected peak values. The calculation results from the measurement points 1-1 and 2-1 are shown in Fig. 25 compared with the direct measurements.

Finally, the axle weights of all the selected train events are calculated. In addition, the errors of the calculated axle

weights are shown in Fig. 25, which are obtained by

$$Error = \frac{(VW_c - VW_m)}{VW_m} \times 100\% \quad (13)$$

where VW_c and VW_m represent the identification results and the direct measurements of axle weights, respectively.

As shown in Fig. 26, the most of relative errors of axle weights were less than 20%. There are several possible reasons: 1) the wheel-force monitoring sensor and the strain gauge are installed at different locations, the dynamic amplification factor of axle weights is changing along the bridge; 2) the average velocities of the axles, instead of instantaneous velocities were used during the correction process of peak values; 3) the static strain components were distorted during the filtering process, as shown in Fig. 5, which may affect the accuracy of the identification results; and 4) according to Eq. (6), axle weights were obtained by distributing the gross train weight, hence, the errors of the calculation results of the gross train weight distributed in axle weights.

5. Conclusions

Accurate identification of moving train loads could

provide reliable information for bridge management and maintenance. In this paper, a classic moving force identification method has been enhanced to handle time-varying velocity of the moving train. The moving train load parameters, including train speed, axle spacing, gross train weight and axle weights, have been identified based on the integral area and the second derivative of the structural strain response. Numerical simulations and measurement results have demonstrated the efficiency and accuracy of the method.

- The proposed method is effective in identifying the moving train load parameters based on the responses of the bridge, and accurate results can be obtained for the train speed, axle spacing and gross train weight. However, the identified axle weights have some errors.

- The most of relative errors of axle weights were less than 20%, which were induced by several possible reasons: 1) the wheel-force monitoring sensor and the strain gauge are installed at different locations; 2) the average velocities of axles were used during the correction process of peak values; 3) the static strain components were distorted during the filtering process; and 4) the errors of the calculation results of the gross train weight distributed in axle weights.

- The time-varying velocities of trains have significant influence on the identification accuracy. In addition, train speeds are increasing slightly when trains pass across the bridge, more attentions should be paid in the analysis.

- Pre-processing procedures are required before the method can work effectively. However, the static strain components are distorted during the process, the peak values of the second derivatives of the strain should be corrected before axle weights calculation.

Acknowledgments

The authors would like to gratefully acknowledge the supports from the National Basic Research Program of China (973 Program) (Grant No. 2015CB060000), the National Natural Science Foundation of China (Grant No. 51722804), the Project of Science and Technology Research and Development Programme of China Railway Corporation (Grant No. 2017G002-K), the National Ten Thousand Talent Program for Young Top-notch Talents (Grant No. W03070080), and the Jiangsu Provincial Key Research and Development Program (Grant No. BE2018120). The authors also thank the help from China Academy of Railway Sciences for providing long-term monitoring data of Xiangtan Bridge.

References

An, Y.H., Guan, D.L., Ding, Y.L. and Ou, J.P. (2017), "Fast warning method for rigid hangers in a high-speed railway arch bridge using long-term monitoring data", *J. Perform. Constr. Fac.*, **31**(6), 04017103.

Catbas, F.N., Zaurin, R., Gul, M. and Gokce, H.B. (2011), "Sensor networks, computer imaging, and unit influence lines for structural health monitoring: case study for bridge load rating", *J. Bridge Eng.*, **17**(4), 662-670.

Chan, T.H., Yu, L., Law, S.S. and Yung, T.H. (2001), "Moving force identification studies, I: theory", *J. Sound Vib.*, **247**(1), 59-76.

Chan, T.H., Yu, L., Law, S.S. and Yung, T.H. (2001), "Moving force identification studies, II: comparative studies", *J. Sound Vib.*, **247**(1), 77-95.

Deng, L. and Cai, C.S. (2010), "Identification of dynamic vehicular axle loads: theory and simulations", *J. Vib. Control*, **16**(14), 2167-2194.

Deng, Y., Liu, Y., Feng, D.M., and Li, A.Q. (2015), "Investigation of fatigue performance of welded details in long-span steel bridges using long-term monitoring strain data", *Struct. Control Health Monit.*, **22**(11), 1343-1358.

Ding, Y.L., Zhao, H.W., Deng, L., Li, A.Q. and Wang, M.Y. (2017), "Early warning of abnormal train-induced vibrations for a steel-truss arch railway bridge: case study", *J. Bridge Eng.*, **22**(11), 05017011.

Doebbling, S.W., Farrar, C.R. and Prime, M.B. (1998), "A summary review of vibration-based damage identification methods", *Shock Vib. Digest*, **30**(2), 91-105.

Gu, Y.M., Li, S.L., Li, H. and Guo, Z.M. (2014), "A novel Bayesian extreme value distribution model of vehicle loads incorporating de-correlated tail fitting: theory and application to the Nanjing 3rd Yangtze River Bridge", *Eng. Struct.*, **59**, 386-392.

Ju, S.H. and Lin, H.T. (2003), "Numerical investigation of a steel arch bridge and interaction with high-speed trains", *Eng. Struct.*, **25**(2), 241-250.

Ju, S.H., Lin, H.T. and Huang, J. Y. (2009), "Dominant frequencies of train-induced vibrations", *J. Sound Vib.*, **319**(1-2), 247-259.

Kim, Y.J. (2012), "Safety assessment of steel-plate girder bridges subjected to military load classification", *Eng. Struct.*, **38**(4), 21-31.

Law, S.S., Bu, J.Q., Zhu, X.Q. and Chan, S.L. (2004), "Vehicle axle loads identification using finite element method", *Eng. Struct.*, **26**(8), 1143-1153.

Law, S.S., Chan, T.H. and Zeng, Q.H. (1997), "Moving force identification: a time domain method", *J. Sound Vib.*, **201**(1), 1-22.

Law, S.S., Chan, T.H. and Zeng, Q.H. (1999), "Moving force identification—a frequency and time domains analysis", *J. Dynam. Syst. Measurement Control*, **121**(3), 394-401.

Long, Y.Q. and Bao, S.H. (2001), *Structural Mechanics*, High Education Press, Beijing, China.

Lu, Y., Mao, L. and Woodward, P. (2012), "Frequency characteristics of railway bridge response to moving trains with consideration of train mass", *Eng. Struct.*, **42**(12), 9-22.

Lydon, M., Taylor, S.E., Robinson, D., Mufti, A. and Brien, E.J.O. (2016), "Recent developments in bridge weigh in motion (B-WIM)", *J. Civil Struct. Health Monit.*, **6**(1), 69-81.

Mao, J.X., Wang, H. and Li, J. (2018), "Fatigue reliability assessment of a long-span cable-stayed bridge based on one-year monitoring strain data", *J. Bridge Eng.*, **24**(1), 05018015.

Mao, J.X., Wang, H., Feng, D.M., Tao, T.Y. and Zheng, W.Z. (2018), "Investigation of dynamic properties of long-span cable-stayed bridges based on one-year monitoring data under normal operating condition", *Struct. Control Health Monit.*, e2146.

Mao, J.X., Wang, H., Xun, Z.X. and Zou, Z.Q. (2017), "Variability analysis on modal parameters of Runyang Bridge during Typhoon Masta", *Smart Struct. Syst.*, **19**(6), 653-663.

Marques, F., Moutinho, C., Hu, W.H., Cunha, Á. and Caetano, E. (2016), "Weigh-in-motion implementation in an old metallic railway bridge", *Eng. Struct.*, **123**, 15-29.

- Milne, D.R.M., Le Pen, L.M., Thompson, D.J. and Powrie, W. (2017), "Properties of train load frequencies and their applications", *J. Sound Vib.*, **397**, 123-140.
- Mori, T., Lee, H.H. and Kyung, K.S. (2007), "Fatigue life estimation parameter for short and medium span steel highway girder bridges", *Eng. Struct.*, **29**(10), 2762-2774.
- Ni, Y.Q., Xia, H.W. and Ko, J.M. (2008), "Structural performance evaluation of Tsing Ma Bridge deck using long-term monitoring data", *Modern Phys. Lett. B*, **22**(11), 875-880.
- Ni, Y.Q., Xia, H.W., Wong, K.Y. and Ko, J.M. (2011), "In-service condition assessment of bridge deck using long-term monitoring data of strain response", *J. Bridge Eng.*, **17**(6), 876-885.
- Ou, J.P. and Li, H. (2010), "Structural health monitoring in mainland China: review and future trends", *Struct. Health Monit.*, **9**(3), 219-231.
- Pan, C.D., Yu, L., Liu, H.L., Chen, Z.P. and Luo, W.F. (2018), "Moving force identification based on redundant concatenated dictionary and weighted l1-norm regularization", *Mech. Syst. Signal Pr.*, **98**, 32-49.
- Spencer Jr, B.F., Moreu, F. and Kim, R.E. (2015), "Campaign monitoring of railroad bridges in high-speed rail shared corridors using wireless smart sensors", Newmark Structural Engineering Laboratory, University of Illinois at Urbana-Champaign.
- Sun, S.W., Sun, L.M. and Chen, L. (2016), "Damage detection based on structural responses induced by traffic load: methodology and application", *Int. J. Struct. Stab. Dynam.*, **16**(4), 1640026.
- Tao, T.Y., Wang, H., Hu, S.T. and Zhao, X.X. "Dynamic behavior of a steel-truss railway bridge under the action of moving trains", *J. Perform. Constr. Fac.*, (Accepted for publication)
- Wang, H., Tao, T.Y., Li, A.Q. and Zhang, Y.F. (2016), "Structural health monitoring system for Sutong cable-stayed bridge", *Smart Struct. Syst.*, **18**(2), 317-334.
- Wang, N.B., Ren, W.X. and He, L.X. (2014), "Extraction of strain influence line of bridge from dynamic responses", *J. Central South Univ.*, **45**(12), 4363-4369.
- Wu, S.Q. and Law, S.S. (2010), "Moving force identification based on stochastic finite element model", *Eng. Struct.*, **32**(4), 1016-1027.
- Xia, H., Zhang, N. and Guo, W.W. (2006), "Analysis of resonance mechanism and conditions of train-bridge system", *J. Sound Vib.*, **297**(3-5), 810-822.
- Xu, Y.L., Chen, B., Ng, C.L., Wong, K.Y. and Chan, W.Y. (2010), "Monitoring temperature effect on a long suspension bridge", *Struct. Control Health Monit.*, **17**(6), 632-653.
- Yang, S.I., Frangopol, D.M. and Neves, L.C. (2004), "Service life prediction of structural systems using lifetime functions with emphasis on bridges", *Reliab. Eng. Syst. Saf.*, **86**(1), 39-51.
- Yu, L. and Chan, T.H. (2007), "Recent research on identification of moving loads on bridges", *J. Sound Vib.*, **305**(1-2), 3-21.
- Yu, Y., Cai, C.S. and Deng, L. (2016), "State-of-the-art review on bridge weigh-in-motion technology", *Adv. Struct. Eng.*, **19**(9), 1514-1530.
- Yu, Y., Cai, C.S. and Deng, L. (2017), "Vehicle axle identification using wavelet analysis of bridge global responses", *J. Vib. Control*, **23**(17), 2830-2840.
- Zaurin, R. and Catbas, F.N. (2009), "Integration of computer imaging and sensor data for structural health monitoring of bridges", *Smart Mater. Struct.*, **19**(1), 015019.
- Zaurin, R. and Necati Catbas, F. (2011), "Structural health monitoring using video stream, influence lines, and statistical analysis", *Struct. Health Monit.*, **10**(3), 309-332.
- Zhao, H., Uddin, N., O'Brien, E.J., Shao, X. and Zhu, P. (2013), "Identification of vehicular axle weights with a bridge weigh-in-motion system considering transverse distribution of wheel loads", *J. Bridge Eng.*, **19**(3), 04013008.
- Zhao, H.W., Ding, Y.L., An, Y.H. and Li, A.Q. (2016), "Transverse dynamic mechanical behavior of hangers in the rigid tied-arch bridge under train loads", *J. Perform. Constr. Fac.*, **31**(1), 04016072.
- Zhu, X.Q. and Law, S.S. (2003), "Identification of moving interaction forces with incomplete velocity information", *Mech. Syst. Signal Pr.*, **17**(6), 1349-1366.
- Zhu, X.Q. and Law, S.S. (2016), "Recent developments in inverse problems of vehicle-bridge interaction dynamics", *J. Civil Struct. Health Monit.*, **6**(1), 107-128.

BS